



This is the accepted manuscript made available via CHORUS. The article has been published as:

Connecting mechanical properties to hydrogen defects in PAN-based carbon fibers

Z. E. Brubaker, S. B. Isbill, A. J. Miskowiec, W. S. Charlton, L. Daemen, and J. L. Niedziela Phys. Rev. Materials **7**, 093603 — Published 14 September 2023

DOI: 10.1103/PhysRevMaterials.7.093603

Connecting mechanical properties to hydrogen defects in PAN-based carbon fibers

Z. E. Brubaker¹, S. B. Isbill¹, A. J. Miskowiec¹, W. S. Charlton², L. Daemen¹, J. L. Niedziela¹

Oak Ridge National Laboratory, Oak Ridge, TN 37831

² University of Texas at Austin, United States

(Dated: August 24, 2023)

Atomic-level defects dictate the mechanical properties of carbon fibers and strong correlations have been established between the crystallite sizes and mechanical properties. We recently demonstrated similar correlations with hydrogen content, but reliably quantifying the hydrogen content is not possible using only inelastic neutron scattering experiments. Here, we present prompt-gamma activation analysis (PGAA) experiments collected on 20 commercially available carbon fibers to quantify the hydrogen content of carbon fibers and find correlations between fiber modulus and hydrogen content. We then evaluate the role of hydrogen defect type and connect the PGAA results to both newly acquired and recently reported inelastic neutron scattering experiments. We find that intercalated hydrogen defects are preferentially removed at carbonization temperatures required for high-modulus fibers, potentially giving rise to voids within the carbon fibers that undermine their tensile strength.

INTRODUCTION

Carbon fibers have emerged as a powerful material class with the potential to replace steels and other materials of construction in applications ranging from the energy and defense sectors, to athletics and automotive industries. One of the primary advantages of carbon fibers is their range of achievable mechanical properties, which can be realized through careful tuning of their manufacturing conditions.

Carbon fibers are composed of graphitic subunits, with a preferred orientation of the basal planes along the fiber axis. The final mechanical properties are dictated by the atomic level defects and degree of orientation, which can be tuned by the final firing temperature, firing times, and strain applied during manufacture [1, 2]. By fine-tuning the strain applied during manufacture, the orientation of the (002) basal planes can be optimized, resulting in larger tensile moduli and strengths. Similarly, by increasing the final firing temperature, atomic-level defects can be removed, resulting in larger crystallite sizes and increased tensile modulus. On the other hand, the tensile strength of PAN-based fibers generally decreases as carbonization temperatures exceed 1,800 K, despite calculations indicating an achievable tensile strength nearly an order of magnitude larger than currently achievable [3–7]. This reduction in tensile strength is likely due to the formation of voids at elevated temperatures, which may arise from gas diffusion through the carbon fiber [1, 5, 8].

Considerable efforts have been dedicated toward understanding the relationship between carbon fiber microstructure, atomic-level defects, and mechanical properties [9–14]. X-ray scattering probes have been used to understand crystallite sizes and the degree of orientation of carbon fibers, and some correlations have been obtained with mechanical properties [9–11]. Because the crystallite size, L_c , has also been observed to be correlated with Raman spectral parameters, significant effort has been made to use Raman spectroscopy to directly probe the fiber modulus and strength [13–17]. Our recent work identified some correlations between the fiber modulus and Raman spectrum, though improving these cor-

relations will be necessary to yield reliable mechanical information from Raman spectra alone [13]. On the other hand, the role of specific defects has remained largely unexplored, but our recent inelastic neutron scattering (INS) experiments demonstrated directional dependence of hydrogen defects, as well as correlations with mechanical properties, though this data set was limited to four fiber types [12].

To explore the role of hydrogen in dictating the mechanical properties of carbon fibers, direct measurements of the hydrogen content are required, but few nondestructive, labscale techniques are sensitive to hydrogen defects contained in carbon fiber systems: the weak Raman-scattering cross sections of hydrogen defects make it difficult to apply Raman spectroscopy to study hydrogen defects, and traditional X-ray based techniques are largely blind to hydrogen because of its low Z-value. Fourier transform infrared (FTIR) spectroscopy data of pure carbon fibers is sparse, and exhibits a number of broad features between 800 and 1,800 cm⁻¹[18–20], though recent FTIR measurements of PAN fibers during stabilization did show several well-defined C–N, C–O, and C–H modes [21].

On the other hand, neutron-based techniques form the goldstandard for studying lighter elements because the large neutron scattering cross section of these elements. Thus, to quantify the hydrogen content and to assess its spatial distribution within carbon fibers, we report prompt-gamma activation analysis (PGAA) and INS experiments, and combine these results with our previous work reporting INS spectra of four fiber types [12]. We demonstrate that the hydrogen concentration decreases with increasing fiber modulus, with highmodulus fibers retaining a small, but finite, amount of residual hydrogen. Informed by INS experiments and computational work [12, 22], we found that the residual hydrogen in highmodulus fibers stems, at least in part, from substituted hydrogen defects, whereas intercalated hydrogen defects are largely absent. These results suggest that intercalated hydrogen defects are preferentially removed at carbonization temperatures necessary for achieving high-modulus fibers. We speculate that specifically diffusion of intercalated hydrogen defects is a source of void and defect formation, thereby reducing the

tensile strength of high-modulus fibers.

MATERIALS AND METHODS

Table I summarizes all fibers and experimental probes discussed. Throughout this manuscript, the material classes are indicated by *SM*, *IM*, and *HM* for *standard* (200–280 GPa), *intermediate* (280–350 GPa), and *high modulus* (>350 GPa).

Although it would be preferable to perform all experiments on unsized carbon fibers, batch dependencies of carbon fibers would undermine connections between PGAA measurements and previously collected data [12, 13, 23, 24]. Thus, to avoid these complicating effects, we elected to measure the same carbon fibers reported in our previous works, recognizing that the fiber sizing may inflate some estimates of the hydrogen content. If the sizing represents 1% mass and if the sizing is primarily composed of bisphenol-A (BPA), then the estimated background from the sizing could be as high as approximately 700 ppm by mass.

That said, a comparison of the sized and unsized T1000 fibers suggests the sizing accounts for 359 \pm 231 ppm H, a smaller value then estimated above. Comparison of the sized and unsized HM fibers similarly suggests that the obtained Hcontent is only somewhat influenced by the fiber sizing. On the other hand, significant differences of the hydrogen content between the three AS4-GP fiber types are observed and potentially result from distinct fiber tows, indicating that other factors (e.g., fiber tow) could have larger effects than fiber sizing. Because we aim to establish connections to our previously collected data and because the effect of sizing appears to be smaller than other complicating factors, we used the same fibers as reported in our other work and made no attempt to remove the fiber sizing. Note, even if the fiber sizing is a larger factor than estimated, six of the seven measured Hexcel fibers contained the same sizing, enabling comparison among these fibers regardless of sizing effects, and many of the measured Toray fibers were unsized.

In the supplemental information, we also show that the INS spectra obtained from BPA—a primary constituent of fiber sizing—cannot account for the peaks attributed to H-defects of carbon fibers in INS spectra, further supporting the fact that sizing is of minimal consequence in this work. [25]

Prompt-gamma activation analysis

The Nuclear Engineering Teaching Laboratory (NETL) at the University of Texas at Austin (UT-Austin) is equipped with a 1.1 MW TRIGA Mark II reactor with an installed guided beam, cold-neutron source at the facility's beam port 3 (BP3). BP3 is used to perform PGAA, which is a nondestructive evaluation technique that allows an analyst to determine the chemical and isotopic constituents of an irradiated sample by analyzing the characteristic gamma-ray radiation emitted

immediately after neutron capture reactions. All elements, except for helium, emit capture gamma-rays that can be detected and used to quantify the element's content within a sample [26]. PGAA can be used for a wide range of nondestructive analytical applications, ranging from low-precision field applications in mineral extraction to highly sensitive laboratory-based techniques. NETL has applied PGAA to a wide range of measurements in materials science, petrochemical research and development, and national security applications [27, 28].

The NETL PGAA system is designed to minimize H background counts and to maximize signal to noise ratio [29]. It utilizes a cold neutron beam line, a solid lead sample chamber purged with helium gas, at least 8 in of lead gamma-ray shielding on all sides, lithium-bearing neutron shielding, and a high-efficiency gamma spectrometer (HPGe) with a Compton suppression system [30]. Samples are placed inside the sample chamber and irradiated for periods up to 8 hours and gamma spectra are collected. This system is energy and efficiency calibrated using a combination of a ¹⁵²Eu decay source standard and measuring the PGAA lines from a thin iron foil. When hydrogen absorbs a neutron, it emits a single 2,223 keV gamma ray which can be recorded by the HPGe detector. The rate of measurement of the 2,223 keV line is proportional to the concentration of hydrogen in the sample. Samples are measured relative to the NIST SRM-2454, hydrogen in titanium alloy, which has a reported hydrogen to titanium mass ratio of 237 ± 6 mg/kg [31].

Prior to measurement, each carbon fiber sample was weighed using a mass balance and baked in a drying oven at 50°C for 16 hours before irradiation to remove any residual moisture. Samples were then placed in a helium-purged sample chamber and measured using the NETL PGAA system for a period of 3-7 hours to acquire sufficient net counts in the 2,223 keV hydrogen line when recorded with two independent, stereoscopic HPGe detectors. Net hydrogen counts ranged from 2,000 to 18,000 counts leading to uncertainties due to counting statistics of between 1% and 10%. Reported uncertainties for each samples included propagation of variance from uncertainties due to hydrogen counts, detector efficiencies, nuclear data, uncertainties in sample mass, and counting uncertainties in the NIST standard. The PGAA measured hydrogen concentration for each sample with estimated uncertainties is shown in Table I.

Inelastic neutron scattering

INS spectra were collected for AS4GP, T800, M46JB, and HM63 fibers using the vibrational spectrometer VISION [32, 33] at the Spallation Neutron Source at Oak Ridge National Laboratory. Fibers were wound (without twisting) around a hollow, borated aluminum plate and secured using aluminum wire, and overwrapped using aluminum foil. The slit sizes were 8×50 mm. As in our previous work [12], the scattering conditions examined were with the incident beam parallel to the plane normal of the sample plate (denoted $\mathbf{k}_i^\perp)$

Fiber	Manufacturer	Sizing	Sizing Mass %	TS GPa	TM GPa	Raman	HT Raman	INS	PGAA H ppm by mass
T700S C	Toray	Unsized	0	4.90	230	[13]	[23, 24]	[12]	$2,232 \pm 38$
AS4-GP	Hexcel	GP	0.8-1.2	4.41	231	[13]	[23]	X	$3,408 \pm 249$
T-300	Cytec	Unsized	0	3.65	231	[13]	[23]	_	$2,\!462\pm322$
AS4C-GP-3k	Hexcel	GP	0.8-1.2	4.39	231	[13]	_		$1,\!662\pm106$
AS4C-GP-12k	Hexcel	GP	0.8-1.2	4.39	231	[13]	_		$2{,}195\pm34$
C C6-4.0/240-T190	Sigrafil	T190	1	4.0	240	[13]	_		$1,\!889\pm32$
KC-14-50k (PX-35)	Zoltek	Sized	Unknown	4.14	241	[13]	_		$1,658 \pm 95$
C T50-4.0/253-E100	Sigrafil	E100	1	4.00	253	[13]	_		$1,450 \pm 169$
T-650/35	Thornel	Epoxy	1	4.27	255	[13]	_	_	$2,\!378\pm110$
C T24-5.0/270-E100	Sigrafil	E100	1	5.00	270	[13]	_		$1,450 \pm 143$
IM7-GP	Hexcel	GP	0.8-1.2	5.65	276	[13]	[23]	[12]	$1,\!457 \pm 47$
IM7Herc	Hercules	Unkown		5.41	276	[13]	_		$1{,}089 \pm 66$
T1000G	Toray	Unsized	0	6.37	294	[13]	_	_	$1,\!684\pm212$
T1000GB-12000-40D	Toray	40D	0.7	6.37	294	[13]	[23]	[12]	$2,043 \pm 44$
T-800	Toray	Sized	0.5-1	5.80	294	[13]	_	X	$1{,}610 \pm 66$
IM10-GP-12K	Hexcel	GP	0.8-1.2	6.96	310	[13]	_		989 ± 92
IM10-GS-12K	Hexcel	GS	0.8-1.2	6.96	310	[13]	[23]	[12]	943 ± 34
M40JB	Toray	Unsized	0	4.41	377	[13]	[23]	_	965 ± 64
M46-JB	Toray	Unsized	0	4.21	436	[13]	[23]	X	637 ± 51
HM63-GP	Hexcel	GP	0.8-1.2	4.69	441	[13]	[23]	X	370 ± 54

TABLE I. Summary of physical and mechanical properties, and other work performed on carbon fibers discussed in this work. "x" denotes new work reported within this manuscript. For completeness, we include references to other experiments performed on these same fiber batches (Raman, Raman of heat-treated fibers, and INS). Fibers that are known to have sizing applied, but the sizing designation is unknown, are labeled as "sized." TS and TM refer to tensile strength and tensile modulus, respectively.

and with the incident beam 75° from the plane normal of the sample plate (denoted \mathbf{k}_i^{75}). The distinction between the experimental configurations is such that the \mathbf{k}_i^{\perp} configuration is sampling the plane perpendicular to the graphitic planes, and the \mathbf{k}_i^{75} configuration is sampling more in plane of the carbon units.

Here, we only discuss the dynamical susceptibility, $\chi''(\mathbf{Q}, E)$, which is a temperature-independent view of the system dynamics. $\chi''(\mathbf{Q}, E)$ is derived from the dynamical structure factor, $S(\mathbf{Q}, E)$, following

$$\chi''(\mathbf{Q}, E) = (1 - \exp(-E/k_BT))S(\mathbf{Q}, E),$$
 (1)

where E is the energy transfer, k_B is the Boltzmann constant, and T is the temperature of the measurement.

Computational work

Carbon fiber sizing is an amorphous polymer with complex structures generally composed of epoxy monomers and curing agents and modeling amorphous materials using computational techniques, such as density functional theory (DFT), can be time consuming. As an approximation, we have modeled the INS spectrum of a BPA-based single crystal using pe-

riodic DFT. The crystal structure of diglycidyl ether of bisphenol A (BPA) [34] was modeled using Vienna Ab initio Simulation Package (VASP 6.1.2) [35-37] on the Compute and Data Environment for Science (CADES) high-performance computing cluster at Oak Ridge National Laboratory. The RPBE exchange-correlation functional [38] was combined with a Γ centered k-point mesh of $2 \times 2 \times 1$ and a plane-wave basis set expanded to a cutoff of 900 eV. The weak interactions between the BPA monomers in the crystal were described using the D3 dispersion method of Grimme with zero damping [39]. Optimization and phonon calculations used Gaussian smearing with a smearing temperature of 0.2 eV. The volume and lattice parameters were held at the experimentally determined values, and atomic positions were relaxed until all forces were less than 0.01 eV/Å and energy changes between steps were less than 10^{-8} eV. Phonons were calculated using the finite displacement method as implemented in Phonopy [40, 41] using VASP to obtain the energies and forces for each displacement. The dynamical matrix calculated with Phonopy using a $4 \times 4 \times 3$ mesh was used to simulate the incoherent contributions to the INS spectrum at 5 K for the VISION spectrometer at the Spallation Neutron Source at Oak Ridge National Laboratory using the O'Climax software [33] for comparison with our previous work [12, 22].

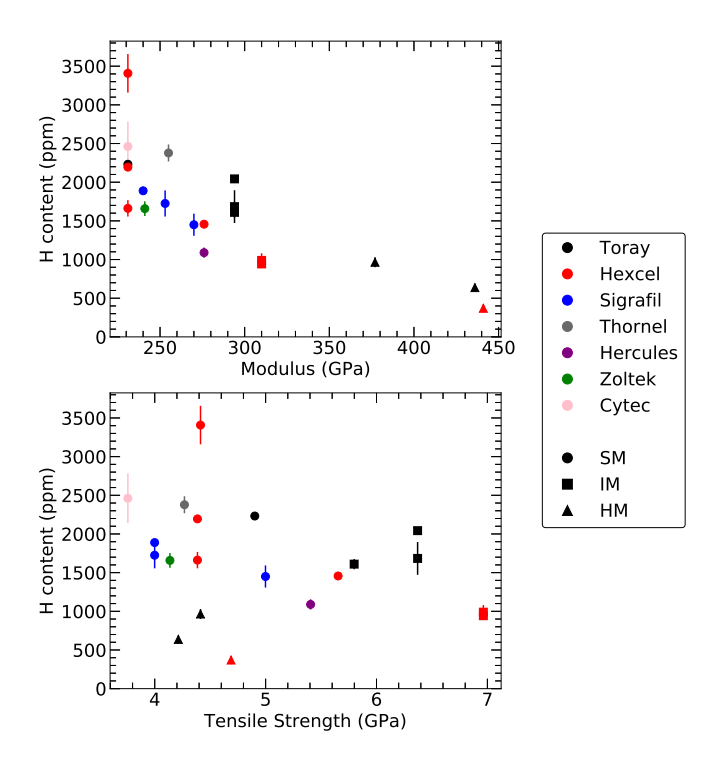


FIG. 1. Hydrogen content plotted against (a) fiber modulus and (b) tensile strength. Circle, square, and triangle markers denote SM, IM, and HM fibers, respectively, and colors indicate manufacturer. The hydrogen content is strongly correlated with fiber modulus, and the lowest hydrogen content was observed for fibers with the largest modulus. On the other hand, the tensile strength of the SM and IM fibers is only weakly correlated with the hydrogen content, with substantial scatter observed throughout. The hydrogen content of the HM fibers is comparable or slightly reduced compared to the highest TS fibers.

RESULTS

Prompt-gamma activation analysis

Previous INS measurements suggested a direct correlation between hydrogen content and thermomechanical properties, but the hydrogen content obtained from INS measurements is inferential, and we could only discuss relative changes in peak intensities [12]. By collecting PGAA data, the hydrogen content of materials can be directly measured [26–28]. Thus, we performed PGAA measurements across 20 commercially available carbon fibers, and plot the obtained hydrogen content as a function of carbon fiber mechanical properties (Fig. 1).

The hydrogen content is strongly correlated with the fiber modulus, with decreasing hydrogen content yielding higher modulus fibers. Especially for a given manufacturer, this qualitative trend is evident. The scatter between manufacturers could feasibly result from concerns about fiber sizing discussed previously, but this may also result from the large number of manufacturing parameters that likely differ between manufacturers.

On the other hand, the hydrogen content is only weakly connected to the carbon fiber tensile strength. For SM and IM fibers, a reduction in hydrogen content appears correlated with increased tensile strength, but significant scatter is observed in the data. Additionally, the HM fibers break this trend: although the hydrogen content of HM fibers is smaller than that observed in SM and IM fibers, their tensile strength is also smaller than the IM fibers.

Interestingly, the HM fibers retain a finite amount of hydrogen, despite the larger carbonization temperatures expected for these fibers compared to SM and IM fibers. We also stress that the M40 and M46 carbon fibers were unsized, suggesting that the residual hydrogen content is not an artifact of fiber sizing. Given the finite hydrogen content of HM fibers, we elected to evaluate the spatial distribution of hydrogen across representative SM, IM, and HM carbon fibers.

Inelastic neutron scattering

To assess the spatial distribution of hydrogen, we present INS data of AS4GP, T800, M46JB, and HM63GP carbon fibers, and supplement it with our previous work studying the INS spectra of T700, IM7, T1000, and IM10 fibers [12]. Figure 2 shows both the newly collected and previously reported INS spectra with the neutron beam along the fiber axis and perpendicular to the fiber axis up to 2,000 cm⁻¹[12]. The supplemental material includes the spectral range up to 3,400 cm⁻¹. All fibers show peaks consistent with those observed for graphite [33], in addition to several additional peaks, such as those near 950 and 1,200 cm⁻¹. Note, all spectra are normalized to the peak near 1,400 cm⁻¹. This normalization was chosen to highlight the distinctions of the peaks near 950 and 1,200 cm^{-1} and is justified by the presence of the peak near 1,400 cm⁻¹ in pure graphite; our previous work normalized to the diffraction peak near 2 Å [12].

Although some distinctions of the graphitic peaks are apparent, the peaks correlated with hydrogen defects are our primary focus. As discussed recently, the peaks near 950 and 1,200 cm⁻¹ correspond to substituted and intercalated hydrogen defects, respectively [22]. Qualitatively, these peaks show the largest intensities for the lower-modulus fibers (T700, AS4GP, IM7GP), and they are reduced in intensity for IM fibers (T800, T1000, IM10GP). For IM10GP and T1000 fibers in the \mathbf{k}_{i}^{75} configurations, the peak near 950 cm⁻¹ is somewhat broad, but a nonzero intensity persists. Critically, the HM fibers retain a finite peak near 950 cm⁻¹, whereas the structure near 1,200 cm⁻¹ is nearly identical to pure graphite. This observation is especially obvious in the \mathbf{k}_{i}^{75} configuration, where the HM fibers and graphite overlap from 1,000 to 1,500 cm⁻¹, implying that intercalated defects are largely absent in HM fibers.

To further ensure that the peaks near 950 and 1,200 cm⁻¹ are not an artifact of fiber sizing or artificially inflated for fibers containing sizing, we evaluated the INS spectra of BPA, which we anticipate is a major component of fiber sizing. Be-

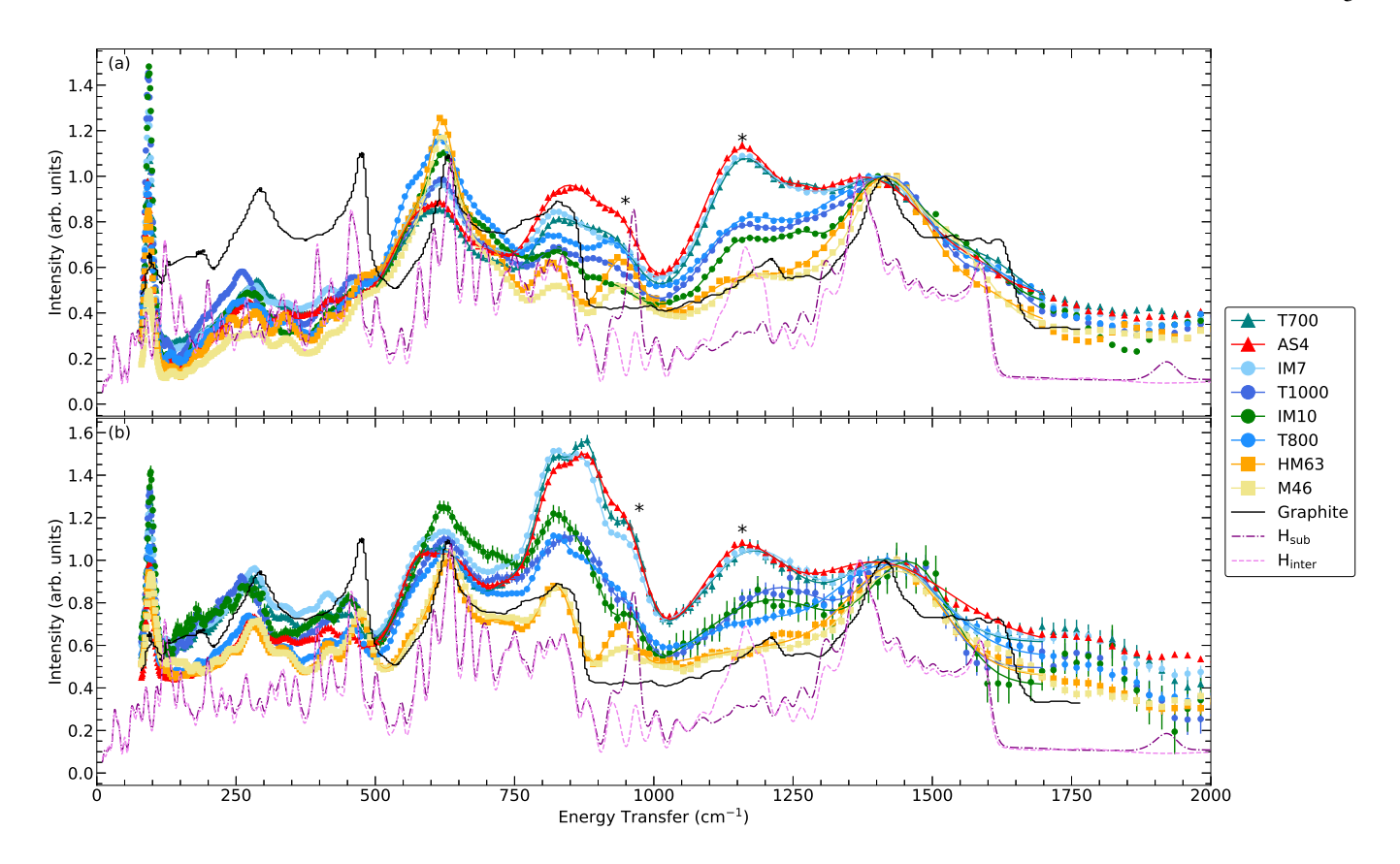


FIG. 2. INS spectra of T700, AS4, IM7, T1000, IM10, T800, M46, and HM63 fibers collected in (top) \mathbf{k}_i^{75} , and (bottom) \mathbf{k}_i^{\perp} configurations. All spectra are normalized to the peak near 1,400 cm⁻¹. The graphite data are reproduced from [33], and the H_{sub} and H_{inter} data are reproduced from [22]. Solid lines between 500 and 1,700 cm⁻¹ represent the obtained fit. Asterisks denote the substituted and intercalated hydrogen defect peaks. The peak intensities near 950 and 1,200 cm⁻¹ are reduced with increasing fiber modulus. Notably, the HM fibers show a complete absence of defect bands near 1,200 cm⁻¹, but they retain a finite contribution from defect bands near 950 cm⁻¹. This observation implies preferential removal of intercalated defects in HM fibers.

cause we are unaware of any experimental INS spectra of BPA up to the wavenumbers considered in this work, we elected to calculate the INS spectra using VASP and O'Climax [33, 35–37]. The results of these calculations are shown in the SI in Fig. S2. [25] BPA shows a number of peaks across the entire spectral range, but the spectral intensity between about 900 and 1,250 cm⁻¹ is relatively flat and cannot account for the peaks we assign as hydrogen-defect peaks. Thus, the residual hydrogen-defect peaks that remain in HM fibers are consistent with the finite hydrogen content observed via PGAA measurements and are unlikely to be a sizing effect.

Quantifying the relative intensities of the 950 and 1,200 cm⁻¹ peaks is challenging. Although pure graphite does not show any significant contribution to neutron scattering intensity near 950 cm⁻¹, substantial overlap and uncertainties result from the peaks closer to 800 cm⁻¹. Further, the spectral intensity observed near 1,200 cm⁻¹ in graphite [33] makes it difficult to confidently extract the spectral contribution only from hydrogen defects, which is exacerbated by the seemingly nonconstant background. Nonetheless, to attempt to quantify the peak intensities, we fit the spectral region between 500 and 1,700 cm⁻¹ using a series of Gaussian

peaks and a constant background; the resulting fits are shown as solid lines in Fig. 2. To estimate the contribution to the peak near 1,200 cm⁻¹ from hydrogen defects, we subtract the peak amplitude determined for pure graphite.

Figure 3 shows the obtained peak amplitudes for the substituted and intercalated bands. The peak amplitudes agree reasonably well with the expectations from the previous qualitative discussion. In general, a decreasing hydrogen content results in a decrease of all hydrogen defect peaks, though the T1000 and T800 fibers (with hydrogen contents near 2,000 and 1,600 ppm, respectively) somewhat break this trend. These fibers show smaller peak amplitudes relative to their hydrogen content. This observation implies that these fibers contain significant quantities of hydrogen outside of the evaluated defects.

DISCUSSION

We now discuss the role of hydrogen in the broader context of carbon fibers. The connection between hydrogen content and fiber modulus provides another observable correlated

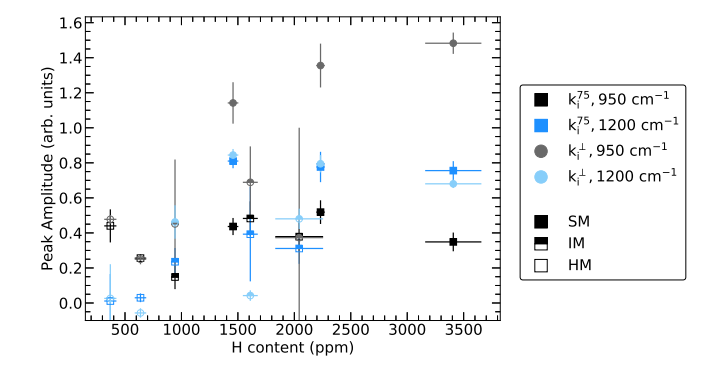


FIG. 3. Peak amplitudes of the substituted (950 cm⁻¹) and intercalated (1,200 cm⁻¹) defects observed in both experimental configurations. Filled, half-filled, and empty markers correspond to SM, IM, and HM fibers, respectively. For the 1,200 cm⁻¹ peaks, the peak amplitude determined for pure graphite has been subtracted [33]. The high-modulus HM63 and M46 fibers (hydrogen contents of 370 and 637 ppm, respectively) retain finite contributions from substituted hydrogen defects, whereas no significant number of intercalated hydrogen defects remain.

with carbon fiber mechanical properties, though it is possible that this correlation results as a byproduct of lower hydrogen content typically accompanying larger crystallite sizes.

Although the connection between hydrogen content and tensile strength is tenuous, the peak in tensile strength of PAN-based carbon fibers near final firing temperatures of 1,800 K may be connected to hydrogen diffusion at elevated temperatures [7]. This peak arises because of the increased presence of voids contained in the carbon fiber matrix [1, 8], which may form as a result of gas diffusion degrading the carbon fiber structure during the carbonization step [5].

A variety of hydrogen desorption mechanisms occur in graphite, and the dominant mechanism is dictated by the exact temperature [42]. Intercalated (physiosorbed) hydrogen is reported to be detrapped between about 900 and 1,300 K in graphite, with higher temperatures being required for chemisorbed hydrogen. Although the substituted hydrogen defects probed in our work do not appear to be directly connected to the chemiosorbed hydrogen in [42], we anticipate that desorption of substituted hydrogen defects would occur at higher temperatures than those required for intercalated hydrogen defects because desorption of substituted hydrogen defects results in a vacancy with dangling bonds. In fact, it has previously been estimated that desorption of hydrogen from vacancies in graphene would require T > 1,200 K [43].

Indeed, our INS results suggest that the higher carbonization temperatures required for HM fibers fully remove intercalated hydrogen defects but leave the substituted defects relatively unperturbed. The desorption of these intercalated defects will involve recombination into H_2 molecules, followed by diffusion throughout the carbon fiber matrix, which could undermine the carbon fiber structure [5, 42]. Thus, targeting a more complete removal of intercalated hydrogen during fiber stabilization may improve the observed tensile strength of HM

fibers.

Separately, we recently reported the Raman spectral response of nine commercially available carbon fibers subject to various heat treatments and found that SM, IM, and HM fibers yielded distinct responses to prolonged exposures in air below 800°C, especially in the spectral region most correlated with the presence of intercalated hydrogen from the DFT work [23]. It is possible that the hydrogen content could elucidate the Raman spectral response of thermally perturbed carbon fibers, but it is unclear if the total hydrogen content or, rather, specific hydrogen defects would be most pertinent. Qualitatively, the SM fibers (T300, AS4GP, T700, IM7) contain the largest hydrogen content and showed larger spectral changes as a function of postproduction heat treatment compared to the IM fibers (T1000, and IM10) implying a connection to hydrogen content. Dedicated studies of the spectral response to postproduction heat treatments of all carbon fibers examined via PGAA would resolve this question, and this work is currently underway.

We also recently reported an analytical model to predict the Raman spectral response of T700 carbon fibers undergoing thermal treatments, and we found that the defect concentration may be the only required quantity to predict the Raman spectral response at arbitrary temperature and treatment time [24]. We are currently assessing whether the hydrogen content could be used to generalize the analytical model across fiber types.

Understanding the quantity and type of hydrogen-defects contained in carbon fibers is essential to understand carbon fibers at a fundamental level. Because of the difficulties Raman and Fourier transform infrared spectroscopy have in reliably obtaining the hydrogen content and defect type, alternate measurements should be considered for extracting this information.

CONCLUSIONS

We measured the hydrogen content of 20 commercially available carbon fibers using PGAA and found a correlation between fiber modulus and hydrogen content. By employing INS, we show that intercalated hydrogen defects predicted from DFT and experimentally evident in lower modulus fibers are absent in HM fibers. We speculate that the diffusion of intercalated hydrogen defects during carbonization of highmodulus fibers is a limiting factor of the tensile strength of PAN-based carbon fibers, and that remnant hydrogen defects in SM and IM fibers are responsible for the degree of spectral changes for those fibers subject to postproduction heat treatment.

ACKNOWLEDGMENTS

This research was funded by the US Department of Energy. A portion of this research used resources at the Spal-

lation Neutron Source, a US Department of Energy Office of Science User Facility operated by Oak Ridge National Laboratory. Z.E.B. conducted the INS experiments with support from L.D., and W.S.C. executed the PGAA measurements. Z.E.B. wrote the manuscript with input from all authors. The authors are grateful to A.E. Shields for assisting with the INS calculations of BPA.

- [1] B. A. Newcomb, Composites, A 91, 262 (2016).
- [2] R. Böhm, M. Thieme, D. Wohlfahrt, D. S. Wolz, B. Richter, and H. Jäger, Fibers 6 (2018).
- [3] S. Chand, Journal of Materials Science 35, 1303 (2000).
- [4] E. Frank, L. M. Steudle, D. Ingildeev, J. M. Spörl, and M. R. Buchmeiser, Angewandte Chemie—International Edition 53, 5262 (2014).
- [5] H. G. Chae and S. Kumar, Science 319, 908 (2008).
- [6] D. C. Papageorgiou, I. A. Kinloch, and R. J. Young, Progress in Materials Science 90, 75 (2017).
- [7] T. Matsumoto, Pure and Applied Chemistry 57, 1553 (1985).
- [8] G. Zhou, Y. Liu, L. He, Q. Guo, and H. Ye, Carbon 49, 2883 (2011).
- [9] S. Kumar, D. Anderson, and A. Crasto, Journal of Materials Science 28, 423 (1993).
- [10] D. Li, H. Wang, and X. Wang, Journal of Materials Science 42, 4642 (2007).
- [11] F. Liu, H. Wang, L. Xue, F. Lidong, and Z. Zhenping, Journal of Materials Science 43, 4316 (2008).
- [12] Z. E. Brubaker, A. Miskowiec, Y. Q. Cheng, L. Daemen, and J. L. Niedziela, Phys. Rev. Materials 6, 013609 (2022).
- [13] Z. E. Brubaker, J. J. Langford, R. J. Kapsimalis, and J. L. Niedziela, Journal of Material Science 56, 1 (2021).
- [14] H. Okuda, R. J. Young, D. Wolverson, F. Tanaka, G. Yamamoto, and T. Okabe, Carbon 130, 178 (2018).
- [15] N. Melanitis, P. L. Tetlow, and C. Galiotis, Journal of Materials Science 31, 851 (1996).
- [16] M. J. Matthews, M. A. Pimenta, G. Dresselhaus, M. S. Dresselhaus, and M. Endo, Physical Review B 59, R6585(R) (1999).
- [17] H. Okuda, R. J. Young, F. Tanaka, J. Watanabe, and T. Okabe, Carbon 107, 474 (2016).
- [18] T. Ohwaki and H. Ishida, Journal of Adhesion 52, 167 (1995).
- [19] T. Ohwaki and H. Ishida, Applied Spectroscopy 49, 341 (1995).
- [20] M. S. de Oliveira Jr., M. F. Diniz, L. Dutra, Rita de Cassia, M. Massi, and C. Otani, Journal of Aerospace Technology and Management 8, 26 (2016).
- [21] S. Nunna, M. Maghe, R. Rana, R. J. Varley, D. B. Knorr, J. M. Sands, C. Creighton, L. C. Henderson, and M. Naebe, Materials 12 (2019), 10.3390/ma12071069.

- [22] S. B. Isbill, Z. E. Brubaker, A. E. Shields, and J. Niedziela, Computational Materials Science 216, 111884 (2023).
- [23] Z. E. Brubaker, A. Miskowiec, and J. L. Niedziela, Phys. Rev. Materials 6, 073603 (2022).
- [24] Z. E. Brubaker, A. Miskowiec, and J. L. Niedziela, Journal of Materials Science 58, 7613 (2023).
- [25] See Supplemental Material at [URL] for the INS spectra across a larger energy transfer range, as well as the calculated INS spectra of BPA.
- [26] R. L. Paul, R. M. Lindstrom, R. R. Greenberg, H. M. P. III, and W. J. Richards, Metallurgical and Materials Transactions A 27, 3682 (1996).
- [27] P. Laine, J. H. Vickery, S. Braun-Sand, D. Dietrich, L. Essman, W. Charlton, C. Alvarado, and J. Lewis, Nuclear Instruments and Methods in Physics Research Section A: Accelerators, Spectrometers, Detectors and Associated Equipment 1045, 167550 (2023).
- [28] W. Charlton, D. Lohmeier, J. Werner, and J. C. Cooley, Transactions of the American Nuclear Society, ANS Annual Meeting, Anaheim, CA, June 12-16, 2022.
- [29] E. J. Artnak, W. S. Charlton, M. J. Andrews, and L. E. Hall, Proceedings of the 2nd International Conference on Radioanalytical and Nuclear Chemistry, Budapest, Hungary, May 5-10, 2019.
- [30] Z. S. Beauvais, W. S. Charlton, M. J. Andrews, and W. M. Payne, MARC XII Conference, Kona, Hawaii, April 3-8, 2022...
- [31] R. L. Paul and R. M. Lindstrom, Metallurgical and Materials Transactions A 43, 4888 (2012).
- [32] S. F. Parker, A. J. Ramirez-Cuesta, and L. Daemen, Spectrochimica Acta Part A 190, 518 (2018).
- [33] Y. Q. Cheng, L. L. Daemen, A. I. Kolesnikov, and A. J. Ramirez-Cuesta, Journal of Chemical Theory and Computation 15, 1974 (2019), pMID: 30735379.
- [34] J. L. Flippen-Anderson and R. Gilardi, Acta Crystallographica Section B 37, 1433 (1981).
- [35] G. Kresse and J. Hafner, Physical Review B 47, 558 (1993).
- [36] G. Kresse and J. Furthmüller, Computational Materials Science 6, 15 (1996).
- [37] G. Kresse and J. Furthmüller, Physical Review B 54, 11169 (1996).
- [38] B. Hammer, L. B. Hansen, and J. K. Nørskov, Phys. Rev. B 59, 7413 (1999).
- [39] S. Grimme, J. Antony, S. Ehrlich, and H. Krieg, The Journal of Chemical Physics 132, 154104 (2010), https://doi.org/10.1063/1.3382344.
- [40] L. Chaput, A. Togo, I. Tanaka, and G. Hug, Phys. Rev. B 84, 094302 (2011).
- [41] A. Togo, L. Chaput, and I. Tanaka, Phys. Rev. B 91, 094306 (2015).
- [42] L. Vergari and R. O. Scarlat, Journal of Nuclear Materials 558, 153142 (2022).
- [43] M. Casartelli, S. Casolo, G. F. Tantardini, and R. Martinazzo, Carbon 77, 165 (2014).